Inorg. Chem. **2008**, *47*, 11154−11165

Inorganic Chemistry

Article

Tricarbonyl Rhenium(I) Complexes Containing a Bridging 2,5-Diphenyl-1,3,4-oxadiazole Ligand: Structural, Spectroscopic, Electrochemical, and Computational Characterization

Matteo Mauro,[†] Monica Panigati,[*,†] Daniela Donghi,[†] Pierluigi Mercandelli,[*,‡] Patrizia Mussini,[§,||] Angelo Sironi,[‡,||,⊥] and Giuseppe D'Alfonso[†,||,⊥]

Dipartimento di Chimica Inorganica, Metallorganica e Analitica (DCIMA) "L. Malatesta", Università di Milano and INSTM, UdR di Milano, via Venezian 21, 20133 Milano, Italy, Dipartimento di Chimica Strutturale e Stereochimica Inorganica (DCSSI), Università di Milano and INSTM, UdR di Milano, via Venezian 21, 20133 Milano, Italy, Dipartimento di Chimica Fisica ed Elettrochimica (DCFE), Università di Milano and INSTM, UdR di Milano, via Golgi 19, 20133 Milano, Italy, Centro di Eccellenza CIMaINa dell'Università di Milano, via Celoria 16, 20133 Milano, Italy, and Istituto di Scienze e Tecnologie Molecolari (ISTM) del CNR, via Golgi 19, 20133 Milano, Italy

Received July 31, 2008

The three complexes $[Re_2(\mu\text{-}X^1)(\mu\text{-}X^2)(CO)_6(\mu\text{-ppd-}\kappa N^3{:}\kappa N^4)]$ (X^1, X^2 = H, **1**; X^1 = H, X^2 = Cl, **2**; X^1, X^2 = Cl, **3**; ppd = 2,5-diphenyl-1,3,4-oxadiazole) have been synthesized by different routes, involving the reaction of $[Re_4(\mu_3\text{-}H)_4(CO)_{12}]$ with ppd for **1**, the reaction of **1** with HCl for **2**, and the reaction of $[ReCl(CO)_5]$ with ppd for **3**. The three complexes possess a different number of valence electrons, so the formal Re−Re bond order varies from 2 to 1 to 0 in complexes **1**, **2**, and **3**, respectively. This is reflected in the Re−Re bond distance (277.9, 297.9, and 358.5 pm in the same series) and in the stability of the complexes in the coordinating solvent acetonitrile ($t_{1/2}$ for ppd displacement 13.6, 4.5, and 3.7 h, for **1**, **2**, and **3**, respectively). Both experimental and calculated structures indicates that coordination induces a distortion from planarity of the diphenyloxadiazole moiety due to the interaction of the equatorial carbonyls with the bridging ppd, which increases on going from **1** to **2** to **3** (dihedral angle between the oxadiazole and the phenyl rings 18.4°, 23.3°, and 45.0°, respectively). The UV spectra show $\pi-\pi^*$ transitions of the oxadiazole ligand (which shift to higher energy on increasing the distortion from the planarity, from 252 to 267 nm) and metal-to-ligand charge transfer absorptions (from 300 to 362 nm). Upon irradiation between 340 and 380 nm, complex **2** only features a weak broad emission at 527 nm (Φ = 0.02%), whereas upon excitation at 300 nm, the emission typical of free ppd is observed, suggesting photodissociation. Cyclic voltammetry investigations in acetonitrile showed that the three complexes exhibit ligand-centered irreversible reduction peaks (from −1.83 to −1.93 V vs $Fc^+|Fc$), shifted to more positive values with respect to free ppd (−2.50 V). The shift however is smaller than in the analogous derivatives containing 1,2-diazines, suggesting a smaller electron depletion of the heterocycle ligand upon coordination. The complexes also show a metal-centered, bielectronic, irreversible oxidation peak (from 1.05 to 1.37 V vs $Fc^+|Fc$). A combined density functional and time-dependent density functional (TD DFT) study allowed us to understand the factors affecting the stability of the three complexes and to rationalize their electrochemical and photophysical properties in terms of their electronic structure.

Introduction

Diaryl-1,3,4-oxadiazoles are electron-poor luminescent molecules, which have been widely investigated as electron transporting materials for optoelectronic devices.[1] Oxadiazole fragments have also been connected to classical chelating ligands (such as bipyridines) in luminescent complexes, to

* To whom correspondence should be addressed. E-mail: monica.panigati@unimi.it (M.P), pierluigi.mercandelli@unimi.it (P.M.). Fax: +39 02 50314405 (M.P), +39 02 50314454 (P.M.). Tel: +39 02 50314352 (M.P.), +39 02 50314447 (P.M.).

† Dipartimento di Chimica Inorganica, Metallorganica e Analitica (DCIMA) "L. Malatesta", Università di Milano and INSTM.

‡ Dipartimento di Chimica Strutturale e Stereochimica Inorganica (DCSSI), Università di Milano and INSTM.

§ Dipartimento di Chimica Fisica ed Elettrochimica (DCFE), Università di Milano and INSTM.

|| Centro di Eccellenza CIMaINa dell'Università di Milano.

⊥ Istituto di Scienze e Tecnologie Molecolari (ISTM) del CNR.

10.1021/ic801447z CCC: $40.75

Published on Web 11/06/2008

Chart 1. Structures of the Three Oxadiazole Complexes Here Investigated, Showing Their Formal Re−Re Bond Order

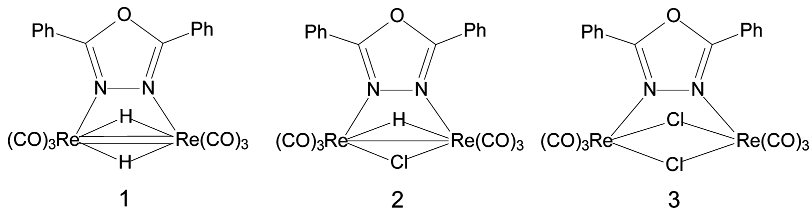

obtain multifunctional (emitting and charge transporting) molecular species.[2] In very few cases, oxadiazoles have been used as ligands by themselves. Complexes of iridium(III) containing chelating cyclometalated (κ^2N,C) oxadiazolates have been reported recently[3−5] and have been tested in the fabrication of electroluminescent devices. Other researchers addressed the use of intact oxadiazoles (containing different substituents on the aryl rings) as rigid bridging ligands in the construction of supramolecular frameworks and reported on several coordination polymers of silver containing the Ag(μ-oxadiazole-κN^3:κN^4)Ag building block.[6]

We turned our attention toward oxadiazoles as ligands on the basis of their similarity to 1,2-diazines, which we have recently used for the preparation of a new family of luminescent tricarbonyl rhenium(I) complexes.[7,8] We have therefore prepared the series of dinuclear rhenium(I) complexes shown in Chart 1, which contain a bridging μ-2,5-diphenyl-1,3,4-oxadiazole-κN^3:κN^4 (ppd) and ancillary ligands (H, Cl) with different steric and electronic properties. Information on the effectiveness of oxadiazole as ligand and on the stability of the complexes on varying the (formal) Re−Re bond order and the Re−Re distance has been obtained. The effect of the coordination on the reduction potential of oxadiazole has been determined and the photophysical properties of the new species have been investigated. The complex stability, the nature of the frontier orbitals, and the electronic transitions involved in the absorption spectrum have been studied by means of density functional and time-dependent density functional calculations.

Scheme 1. The Synthetic Routes to the Novel Oxadiazole Complexes **1**, **2**, and **3**

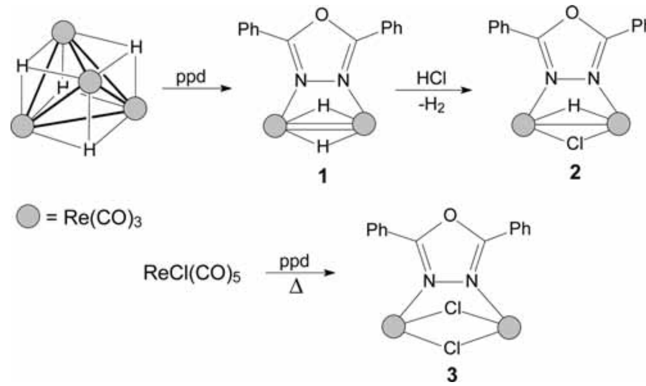

Results and Discussion

Syntheses of the New Complexes. Different pathways have been followed for the synthesis of the [$Re_2(\mu$-$X^1)(\mu$-$X^2)(CO)_6(\mu$-ppd-κN^3:$\kappa N^4)$] complexes (X^1, X^2 = H, Cl; ppd = 2,5-diphenyl-1,3,4-oxadiazole), as summarized in Scheme 1. In all cases, the nature of the products has been established on the basis of the spectroscopic data and confirmed by single-crystal X-ray diffractometric analysis.

The dinuclear hydrido complex [$Re_2(\mu$-$H)_2(CO)_6(\mu$-ppd)] (**1**) was obtained in high yields by a route analogous to that used for the synthesis of the corresponding pyridazine derivative [$Re_2(\mu$-$H)_2(CO)_6(\mu$-pydz-κN^1:$\kappa N^2)$] (pydz = pyridazine),[7] namely, the reaction of the unsaturated tetrahedral cluster [$Re_4(\mu_3$-$H)_4(CO)_{12}$] with 2 equiv of ppd at room temperature in dichloromethane solution. NMR monitoring revealed complete disappearance of the starting cluster in about 4 h to give mainly the dinuclear complex **1**, which is poorly soluble in dichloromethane and slowly precipitates from the reaction mixture (isolated yield ca. 70%).[9]

The mixed hydridochloro complex [$Re_2(\mu$-H)(μ-Cl)$(CO)_6(\mu$-ppd)] (**2**) was prepared by reaction of **1** with a saturated dichloromethane solution of gaseous HCl, according to eq 1. The reaction was selective and went to completeness in about 4 h at room temperature.

(1) (a) Shirota, Y.; Kageyama, H. *Chem. Rev.* **2007**, *107*, 953–1010. (b) Kulkarni, A. P.; Tonzola, C. J.; Babel, A.; Jenekhe, S. A. *Chem. Mater.* **2004**, *16*, 4556–4573.
(2) Si, Z.; Li, J.; Li, B.; Zhao, F.; Liu, S.; Li, W. *Inorg. Chem.* **2007**, *46*, 6155–6163. (b) Wong, Y. P.; Xie, W. F.; Li, B.; Li, W. L. *Chin. Chem. Lett.* **2007**, *18*, 1501–1504. (c) Liu, C. B.; Li, J.; Li, B.; Hong, Z. R.; Zhao, F. F.; Liu, S. Y.; Li, W. L. *Chem. Phys. Lett.* **2007**, *435*, 54–58. (d) Lundin, N. J.; Blackman, A. G.; Gordon, K. C.; Officer, D. L. *Angew. Chem., Int. Ed.* **2006**, *45*, 2582–2584. (e) Xiang, N. J.; Leung, L. M.; So, S. K.; Wang, J.; Su, Q.; Gong, M. L. *Mater. Lett.* **2006**, *60*, 2909–2913. (f) He, Z.; Wong, W.-Y.; Yu, X.; Kwok, H.-S.; Lin, Z. *Inorg. Chem.* **2006**, *45*, 10922–10937. (g) Wong, W.-Y.; He, Z.; So, S.-K.; Tong, K.-L.; Lin, Z. *Organometallics* **2005**, *24*, 4079–4082. (h) Ng, P. K.; Gong, X.; Chan, S. H.; Lam, L. S. M.; Chan, W. K. *Chem.—Eur. J.* **2001**, *7*, 4358–4367. (i) Kim, Y.; Vanhelmont, F. W. M.; Stern, C. L.; Hupp, J. T. *Inorg. Chim. Acta* **2001**, *318*, 53–60. (j) Gong, X.; Ng, P. K.; Chan, W. K. *Adv. Mater.* **1998**, *10*, 1337–1340.
(3) (a) Chen, L.; You, H.; Yang, C.; Ma, D.; Qin, J. *Chem. Commun.* **2007**, 1352–1354. (b) Chen, L.; Yang, C.; Li, M.; Qin, J.; Gao, J.; You, H.; Ma, D. *Cryst. Growth Des.* **2007**, *7*, 39–46.
(4) An aluminum derivative, analogous to Alq_3, had been reported some times ago, which contains a κ^2N,O cyclometalated phenolate oxadiazole: Wang, J. F.; Jabbour, G. E.; Mash, E. A.; Anderson, J.; Zhang, Y.; Lee, P. A.; Armstrong, N. R.; Peyghambarian, N. *Adv. Mater.* **1999**, *11*, 1266–1269.
(5) A cyclomanganated complex has also been reported: Michon, C.; Djukic, J.-P.; Pfeffer, M.; Gruber-Kyritsakas, N.; De Cian, A. *J. Organomet. Chem.* **2007**, *692*, 1092–1098.
(6) (a) Dong, Y.; Xu, H.; Ma, J.; Huang, R. *Inorg. Chem.* **2006**, *45*, 3325–3343. (b) Dong, Y.; Zhang, Q.; Wang, L.; Ma, J.; Huang, R.; Shen, D.; Chen, D. *Inorg. Chem.* **2005**, *44*, 6591–6608.
(7) Panigati, M.; Donghi, D.; D'Alfonso, G.; Mercandelli, P.; Sironi, A.; D'Alfonso, L. *Inorg. Chem.* **2006**, *45*, 10909–10921.
(8) Donghi, D.; D'Alfonso, G.; Mauro, M.; Panigati, M.; Mercandelli, P.; Sironi, A.; Mussini, P.; D'Alfonso, L. *Inorg. Chem.* **2008**, *47*, 4243–4255.

$$[Re_2(\mu\text{-}H)_2(CO)_6(\mu\text{-ppd})] + HCl \rightarrow [Re(\mu\text{-}H)(\mu\text{-}Cl)(CO)_6(\mu\text{-ppd})] + H_2 \quad (1)$$

The dichloro derivative $[Re_2(\mu\text{-}Cl)_2(CO)_6(\mu\text{-ppd})]$ (**3**) was obtained in high yield by treating $[ReCl(CO)_5]$ with 0.5 equiv of ppd in toluene at reflux. Also in this case, the synthesis parallels that of the analogous 1,2-diazine derivatives recently reported.[8] Spectroscopic analysis (IR and NMR) of the reaction mixture assessed the good selectivity of the reaction.

The three complexes **1**, **2**, and **3** possess 32, 34, and 36 valence electrons, respectively. Accordingly, the formal Re−Re bond order varies from 2 to 1 to 0 in the same series, as evidenced in Chart 1. This is reflected in the Re−Re distance (see below) and in the stability of the complexes.

Actually, the three complexes have been found to be rather unstable in acetonitrile solution. In all cases, ^{1}H NMR monitoring showed loss of the oxadiazole ligand following a clean pseudo-first-order behavior with a rate that decreased on increasing the formal Re−Re bond order: $t_{1/2} = 3.7$, 4.5, and 13.6 h, for **3**, **2**, and **1**, respectively. The reaction products, only partially identified, were different in the three cases. For **3**, the reaction resulted in fragmentation of the dinuclear unit, according to eq 2, with formation of the mononuclear complex $[ReCl(CO)_3(MeCN)_2]$, identified by its ν(CO) IR bands.[10]

$$[Re_2(\mu\text{-}Cl)_2(CO)_6(\mu\text{-ppd})] + 4MeCN \rightarrow 2[ReCl(CO)_3(MeCN)_2] + ppd \quad (2)$$

In contrast, in the case of the reaction of **2** with acetonitrile, the dinuclear skeleton was maintained, as the ^{1}H NMR monitoring showed that the main product exhibited a resonance unambiguously attributable to a bridging hydrido ligand (δ −9.13 ppm). This species has been tentatively formulated as $[Re_2(\mu\text{-}H)(\mu\text{-}Cl)(CO)_6(MeCN)_2]$, on the basis of its spectroscopic data.[11]

In the case of **1**, its very slow decomposition in acetonitrile-d_3 was poorly selective and led to the progressive formation of a number of hydrido species, as well as to H_2 evolution, as described in more detail in the Experimental Section.

The lability of the dinuclear structure in the case of **3** was further evidenced by its decomposition (with oxadiazole loss) even in a less donating solvent such as tetrahydrofuran, with a longer $t_{1/2}$ than in acetonitrile (17 h).

The relatively fast decomposition of **3** in acetonitrile compared with the stability in the same conditions of the related $[Re_2(\mu\text{-}Cl)_2(CO)_6(\mu\text{-pydz})]$ derivative suggests that ppd is a worse ligand than 1,2-diazine, in line with its lower basicity (pK_a values −2.49 for ppd[14] vs +2.33 for pydz[15]). The preference of rhenium for binding to pyridazine has been confirmed by a competition experiment, in which a toluene solution of $[ReCl(CO)_5]$ was refluxed in the presence of 0.5 equiv of ppd and of pydz. The NMR spectra showed the almost quantitative formation of the diazine derivative.

It is also worthwhile to mention that **3** was the only reaction product even when $[ReCl(CO)_5]$ was treated with 1 equiv (or more) of ppd, unlike the analogous reaction with pyridazine, which under these conditions affords the mononuclear species *fac*-$[ReCl(CO)_3(pydz)_2]$, containing two monodentate diazine ligands.[8,16]

Structural Characterization. The structures of the complexes **1**−**3** have been established by single-crystal X-ray analysis.[17] Figure 1 shows a picture of the three species, and Table 1 reports some relevant geometrical parameters, averaged according to the idealized C_s symmetry of these molecules. Each rhenium atom attains a distorted octahedral coordination and bears three terminal carbonyl ligands (in a facial arrangement), two bridging (hydrido or chloro) ligands, and one of the nitrogen atoms of the bridging 2,5-diphenyl-1,3,4-oxadiazole ligand. The Re−Re distance observed in the three species (277.9, 297.9, and 358.5 pm in **1**, **2**, and **3**, respectively) is in agreement with their (formal) Re−Re bond order (2, 1, and 0, respectively) and with the dimension of the bridging hydrido or chloro ligands.

The molecular structures of **1** and **3** are strictly related to those of the corresponding all-carbonyl derivatives $[Re_2(\mu\text{-}H)_2(CO)_8]$ and $[Re_2(\mu\text{-}Cl)_2(CO)_8]$.[18] The bridging coordination of an oxadiazole molecule leads, however, to major structural perturbations. Indeed, to allow the lone pairs on the two nitrogen atoms to effectively interact with the metal atoms, the two rhenium-centered octahedra must bend toward the bridging ligand, leading to a larger Re−Re−C^{ax} angle (+5.6° and +22.2° for **1** and **3**) and to a shorter Re−Re distance (−9.7 and −22.9 pm for **1** and **3**) with respect to the D_{2h}-symmetric all-carbonyl species.

(9) The ^{1}H NMR analysis (in THF-d_8) of the lemon yellow precipitate revealed that it was constituted by complex **1** only. Contrary to what occurred in the reaction with pyridazine, no tetranuclear clusters with spiked-triangular skeleton have been detected as intermediates. At further variance, the tetranuclear square clusters, which were the main products in the reactions with pyridazine, in this case were formed only in traces. The main byproducts (less than 5%) of the reaction with ppd have been identified, on the basis of their NMR signals, as the *cis* and *trans* isomers (ratio ca. 1:2) of the triangular cluster $[Re_3(\mu\text{-}H)_3(CO)_9(\mu\text{-ppd})(\text{ppd-}\kappa N^3)]$. The formulation of these byproducts has been confirmed by their preparation through the reaction of the triangular cluster $[Re_3(\mu_3\text{-}H)(\mu\text{-}H)_3(CO)_9]^-$ with CF_3SO_3H in the presence of 2 equiv of ppd. A full characterization of these species and the study of their properties are in progress.

(10) Farona, M. F.; Kraus, K. F. *Inorg. Chem.* **1970**, *9*, 1700–1704.

(11) Particularly diagnostic was the position of its hydrido resonance. Indeed, the analogous $[Re_2(\mu\text{-}H)(\mu\text{-}Cl)(CO)_8]$ complex gives a hydrido signal at −12.7 ppm,[12] and it has been previously observed that the replacement of carbonyls by MeCN molecules in a $(CO)_4Re(\mu\text{-}H)Re(CO)_4$ fragment causes a strong downfield shift of the hydrido resonance.[13]

(12) Adams, R. D.; Kuhns, J. D. *Polyhedron* **1988**, *7*, 2543–2547.
(13) Beringhelli, T.; D'Alfonso, G.; Freni, M.; Ciani, G.; Sironi, A.; Molinari, H. *Dalton Trans.* **1986**, 2691–2697.
(14) Trifonov, R. E.; Rtishchev, N. I.; Ostrovskii, V. A. *Spectrochim. Acta, Part A* **1996**, *52*, 1875–1882.
(15) Dean, J. A. *Lange's Handbook of Chemistry*; McGraw-Hill: New York, 1992.
(16) Abel, E. W.; Blackwall, E. S.; Heard, P. J.; Orrel, K. G.; Sik, V.; Hursthouse, M. B.; Mazid, A. M.; Abdul Malik, K. M. *Dalton Trans.* **1994**, *100*, 445–455.

(17) CCDC-695237−95239 contain the crystallographic data for **1**−**3**. These data can be obtained free of charge from The Cambridge Crystallographic Data Centre (www.ccdc.cam.ac.uk).

(18) (a) Masciocchi, N.; Sironi, A.; D'Alfonso, G. *J. Am. Chem. Soc.* **1990**, *112*, 9395–9397. (b) Vega, A.; Calvo, V.; Manzur, J.; Spodine, E.; Saillard, J.-Y. *Inorg. Chem.* **2002**, *41*, 5382–5387.

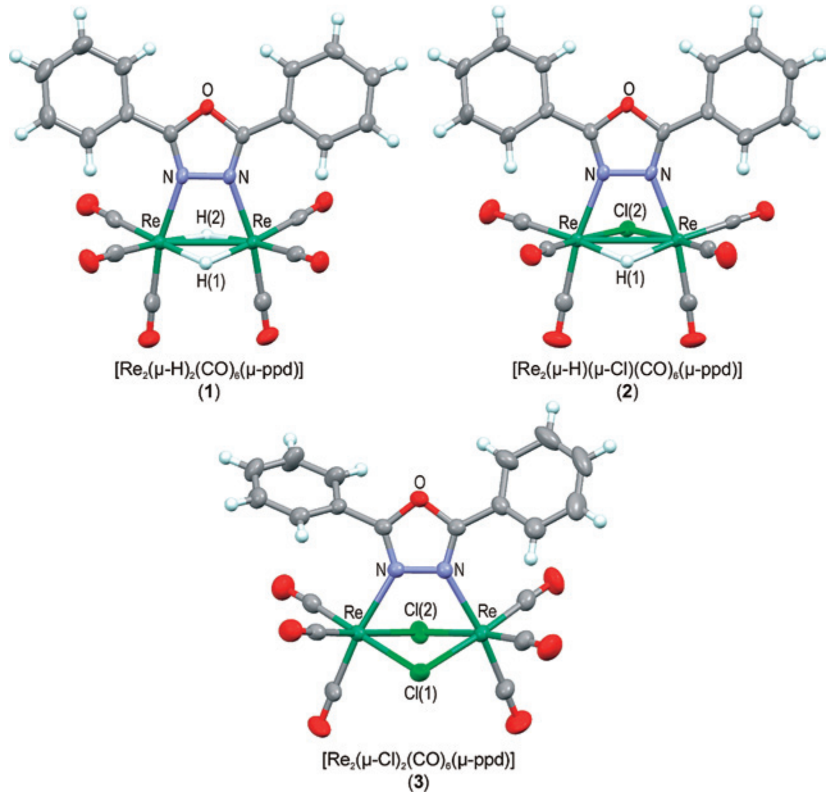

Figure 1. View of the molecular structure of the three $[Re_2(\mu\text{-}X^1)(\mu\text{-}X^2)(CO)_6(\mu\text{-ppd})]$ species, as determined by X-ray diffraction, with a partial labeling scheme.

Table 1. Experimental and Calculated Geometrical Parameters [pm and deg] for the Complexes $[Re_2(\mu\text{-}X^1)(\mu\text{-}X^2)(CO)_6(\mu\text{-ppd})]$ (**1**−**3**)[a]

	exptl			calcd		
	1	**2**	**3**	**1**	**2**	**3**
Re−Re	277.89(7)	297.92(9)	358.48(8)	280.8	300.7	361.3
Re−X^1	185.3	185.2	249.06(11)	188.0	185.7	252.0
Re−X^2	185.4	249.52(9)	249.85(11)	189.0	252.9	253.5
Re−N	219.0(9)	219.6(2)	222.0(3)	221.8	221.8	224.6
N−N	140.6(5)	141.5(3)	141.4(4)	138.4	138.2	138.5
Re−N−N	108.3(2)	110.86(14)	118.9(2)	108.7	111.5	119.7
Re−Re−C^{ax}	97.67(15)	100.6(2)	111.49(11)	98.4	101.2	111.8
eq^1/eq^2	18.1	20.8	38.06(10)	15.6	20.1	39.6
C_2N_2O/Ph	18.4(3)	23.34(15)	45.0(2)	17.3	28.0	43.4

[a] For **1**, $X^1 = X^2 = H$; for **2**, $X^1 = H$ and $X^2 = Cl$; for **3**, $X^1 = X^2 = Cl$. C_2N_2O and Ph are the least-squares planes defined by the oxadiazole five-membered ring and the phenyl ring, respectively; eq^1 and eq^2 are the planes defined by the equatorial ligands of the two rhenium atoms. Numbers in parentheses are the greatest standard uncertainties on individual values. Further geometrical parameters are listed in Table S1 (Supporting Information).

An interesting feature of these species is the distortion from planarity of the 2,5-diphenyloxadiazole moiety. Indeed, as a consequence of the interaction of the equatorial carbonyl ligands with the bridging heterocycle, the two phenyl rings rotate in the same direction out of the plane of the oxadiazole ring. The effect increases on going from **1** to **2** to **3**, as shown by the dihedral angle between the planes defined by the oxadiazole five-membered ring and the phenyl ring (C_2N_2O/Ph 18.4°, 23.3°, and 45.0°), in agreement with the increase of the bending of the rhenium-centered octahedra, as measured by the Re−Re−C^{ax} angle (97.7°, 100.6°, and 111.5°) and by the dihedral angle between the planes defined by the equatorial ligands of the two rhenium atoms (eq^1/eq^2 18.1°, 20.8°, and 38.1°). This rotation of the phenyl rings leads to a progressive loss of conjugation within the 2,5-diphenyl-1,3,4-oxadiazole ligand and, in the case of **1** and **3**, to a reduction of the idealized symmetry of the molecule from C_{2v} to C_s.[19]

Table 2. Absorption Data for the Complexes $[Re_2(\mu\text{-}X^1)(\mu\text{-}X^2)(CO)_6(\mu\text{-ppd})]$ (**1**−**3**) in Dichloromethane Solution at RT

	λ_{abs} (ε) [nm (10^3 M^{-1} cm^{-1})]	
	$\pi-\pi^*$	^{1}MLCT
ppd	283 (30)	
1	267 (31)	362 (11)[a]
2	261 (34)	300 (16)
3	252 (27)	n.d.[b]

[a] Partially overlapped less intense absorptions are observed at 310 and 416 nm. [b] The position of the band cannot be established with certainty (see Figure 2).

Photophysical Characterization. The absorption spectra of **1**, **2**, and **3** in dichloromethane solution show, in the UV range, one band (at 267, 261, and 253 nm, respectively) attributable to the intraligand $\pi-\pi^*$ transition of the oxadiazole molecule (See Table 2 and Figure 2). These absorptions are blue-shifted with respect to the free oxadiazole molecule (283 nm)[20] by 16, 22, and 30 nm, respectively. This shift can be attributed to a conformational twist of the dihedral angle between the phenyl groups and the oxadiazole

(19) For the dichloro derivative **3**, the two C_2N_2O/Ph dihedral angles are significantly different, 61.6(2)° and 28.3(2)°, as can be noticed in Figure 1. However, all the remaining geometrical parameters are consistent with an overall idealized C_s-symmetrical structure, as confirmed by the computational study.

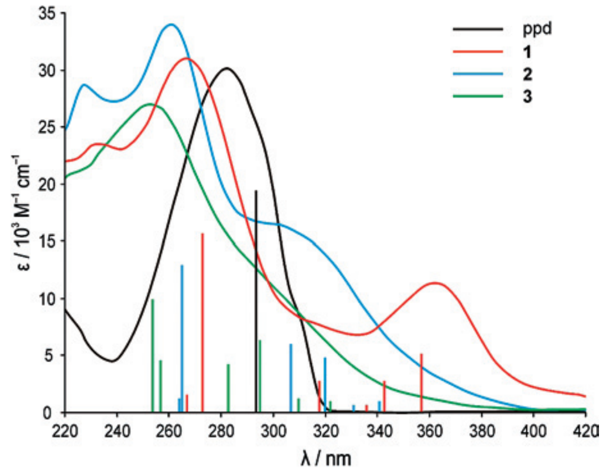

Figure 2. Absorption spectra (normalized with respect to the $\pi-\pi^*$ transition) of the three complexes $[Re_2(\mu\text{-}X^1)(\mu\text{-}X^2)(CO)_6(\mu\text{-ppd})]$ (**1**−**3**) and the free ligand (ppd) in dichloromethane solution. A comparison with excitation energies and oscillation strengths computed in dichloromethane is reported (vertical lines).

ring, induced by the coordination to the metal, as discussed in the structural and computational part of this work.[21]

Complex **1** shows another main absorption, at lower energy (362 nm), which can be assigned to a metal-to-ligand charge transfer transition (^{1}MLCT). Indeed, on increasing solvent polarity, the position of the band shifts to higher energy (from 367 nm in toluene to 357 nm in ethanol), as is typical of charge transfer transitions,[22] while the position of the band attributed to the $\pi-\pi^*$ transition remains unchanged. For complexes **2** and **3**, these charge transfer bands are significantly blue-shifted and fall on the tail end of the intraligand $\pi-\pi^*$ transition: the charge transfer band of **2** is still recognizable, at ca. 300 nm (Figure 2), while that of **3** is almost completely buried and appears as a broad tail of the higher energy absorption. Density functional calculations (see below) support this view.

The photoluminescent behavior of the three complexes was investigated at room temperature in toluene solution. No emission was observed for **1** and **3** upon irradiation at wavelengths in the range 340−380 nm. In contrast, for complex **2** a weak broad emission was observed at 527 nm (Φ = 0.02%) upon irradiation at 370 nm. The large Stokes shift agrees with an emission from a ^{3}MLCT state.

When the excitation wavelength was shifted to 300 nm, for all the complexes a structured emission appeared (λ_{max} = 348 nm). Its position and shape were however identical to that of the free ppd ligand. This suggests that the complexes are unstable in solution under UV irradiation and dissociate the oxadiazole ligand. Actually, a progressive neat increase of the emission intensity was observed in a series of spectra acquired sequentially (as shown for **3** in Figure S1 of Supporting Information).

Electrochemical Characterization. The three complexes **1**, **2**, and **3** and the free ligand ppd have been investigated by cyclic voltammetry (CV), and the most significant results are summarized in Table 3 and Figure 3.

Ligand. The oxadiazole ligand features a series of reduction peaks in the potential window available in the chosen medium (acetonitrile containing 0.1 M tetrabutylammonium hexafluorophosphate, $TBAPF_6$). The first peak in the series appears to be chemically and electrochemically reversible and monoelectronic, consistent with the 57 mV half-peak width, the nearly zero slope of the E_p vs log v linear characteristics (where v indicates the scan rate), and the presence of a symmetrical return peak. Such a peak clearly corresponds to the formation of a stable radical anion and strongly resembles (both in potential and features, see Table 3 and Figure 3) the case of the ligand phthalazine (phal) studied in our previous work concerning the rhenium complexes with 1,2-diazines.[8] Interestingly, it has been previously shown that the ligand pyridazine, featuring a less extended π-system than phthalazine or diphenyloxadiazole, gives a bielectronic, chemically irreversible first reduction peak, corresponding to an ECE mechanism.[8,23]

The normalized current for ppd (Figure 3) is lower than both the normalized phthalazine and ferrocene ones under the same conditions, indicating a lower diffusion coefficient of the oxadiazole molecule.

Complexes. First Reduction Peak. The first reduction peaks of complexes **1**−**3** are still ligand-centered, as demonstrated by their appearance almost unchanged on varying the nature of the monatomic bridging ligands.[24] The peak potentials are shifted to more positive values with respect to free ppd, as a consequence of the electron donation to the rhenium atoms. However, this shift (0.56 V for **3**) is much less pronounced than in the analogous pyridazine (1.26 V) and phthalazine (0.93 V) derivatives,[8] suggesting a smaller electron depletion of the heterocycle ligand upon coordination, thus a less efficient electron donation.

Upon complexation, the first reduction peak of oxadiazole loses its chemical reversibility, showing that the radical anion undergoes a fast chemical step in the experimental time scale. This again resembles what was observed in the phthalazine case (Figure 3),[8] and it is quite the opposite of the pyridazine case, where the chemically irreversible, bielectronic reduction peak of the free ligand becomes a monoelectronic, chemically reversible peak upon complexation.[8]

Complexes. First Oxidation Peak. The first oxidation peaks of the three complexes are clearly metal-centered, as demonstrated by the variation of the peak potentials on varying the nature of the monatomic ligands X^1 and X^2. They also appear to be bielectronic, like the first oxidation peaks of the pyridazine and phthalazine complexes.[8] However, different from the latter case, where electrochemically and chemically revers-

(20) Ballard, R. E.; Titchard, A. *Spectrochim. Acta, Part A* **1967**, *23*, 1883–1887.
(21) See also: Jansson, E.; Jha, P. C.; Ågren, H. *Chem. Phys.* **2006**, *330*, 166–171.
(22) (a) Drago, R. S. *Physical Methods in Chemistry*; W. B. Saunders Company: Philadelphia, PA, 1977. (b) Giordano, P. J.; Wrighton, M. S. *J. Am. Chem. Soc.* **1979**, *101*, 2888–2897, and references therein.
(23) *Organic Electrochemistry*, 4th ed.; Lund, H., Hammerich, O., Eds.; Dekker: New York, 2001; pp 695−696, and references therein.
(24) Moreover, the very small variation of the reduction potentials with increasing ligand electronegativity is contrary to the trend expected from the inductive effect of the hydrido and chloro ligands, confirming that metal orbitals are not involved in the reduction.

Table 3. Selected CV Features Obtained for the Free Diphenyloxadiazole Ligand (ppd) and Its Rhenium Complexes $[Re_2(\mu\text{-}X^1)(\mu\text{-}X^2)(CO)_6(\mu\text{-ppd})]$ (**1**−**3**)[a]

	first reduction peak				first oxidation peak				
ligands and complexes	$E_{p,cI}$ [V]	$\lvert E_p - E_{p/2}\rvert$ [V]	$\lvert dE_p/d \log v\rvert$ [V]	$i_{L,conv}/c$ [A cm^{-2} mol^{-1} dm^3]	$E_{p,aI}$ [V]	$E_p - E_{p/2}$ [V]	$dE_p/d \log v$ [V]	$i_{L,conv}/c$ [A cm^{-2} mol^{-1} dm^3]	E_g [eV]
ppd	−2.495	0.057	0.005	0.41					
1	−1.827	0.043	0.027	0.47	1.045	0.054	0.033	0.69	2.87
2	−1.898	0.043	0.021	0.53	1.175	0.108	0.081	1.17	3.07
3	−1.932	0.056	0.033	0.52	1.374	0.049	0.016	0.58	3.31
phal	−2.458	0.054	0.006	0.51					
3phal	−1.532	0.040	0.023	0.34	1.244	0.030	0.010	0.61	2.78

[a] Scan rate 0.2 V s^{-1}, performed in MeCN with 0.1 M $TBAPF_6$ as the supporting electrolyte, at 298 K, with ohmic drop compensation. First cathodic and anodic peak potentials ($E_{p,cI}$ and $E_{p,aI}$), together with relevant half-peak widths ($E_p - E_{p/2}$), slopes of the linear E_p vs log v characteristics (dE_p/d log v), normalized limiting currents after convolution ($i_{L,conv}/c$),and electrochemical energy gaps (E_g). Potentials are referred to the Fc^+|Fc couple in the operating medium. Data for phthalazine (phal) and its dichloro rhenium complex (**3phal**) are taken from ref 8.

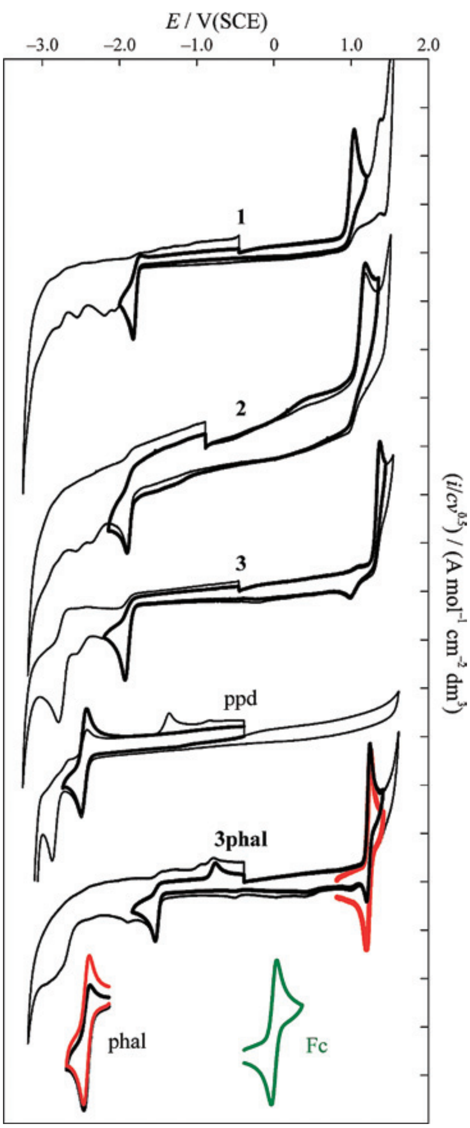

Figure 3. A synopsis of normalized CV characteristics obtained for ppd and its rhenium complexes (**1**−**3**) at 0.2 V s^{-1} scan rate in MeCN with 0.1 M $TBAPF_6$ as the supporting electrolyte, at 298 K, with ohmic drop compensation. Normalized CV features for phthalazine (phal), its complex **3phal**, and the reference redox couple Fc^+|Fc, obtained in the same conditions, are also reported. Red curves have been obtained at 2 V s^{-1}.

ible two-electron transfer was observed, the peaks of the oxadiazole complexes are wider and show a significant negative shift with increasing scan rate, indicating less facile electron transfer (particularly in the case of **2**). Moreover, no return peak is observed in the experimental time scale, pointing to a fast chemical step following the electron transfer, as in the case of the reduction peak.[25]

Comparison between the electrochemical behavior of **3** and that of **3phal** (Table 3 and Figure 3) shows that for the phthalazine complex **3phal** both reduction and oxidation are easier than for the corresponding ppd complex **3** (by 0.40 and 0.13 V, respectively), resulting in a significantly lower HOMO−LUMO gap. Both features can be explained by the less efficient ligand-to-metal electron donation from the oxadiazole, resulting in a ring richer in electrons and a metal redox site poorer in electrons with respect to the phthalazine case.

Computational Study. The three oxadiazole rhenium complexes $[Re_2(\mu\text{-}X^1)(\mu\text{-}X^2)(CO)_8(\mu\text{-ppd})]$ (**1**−**3**) have been studied by means of density functional and time-dependent density functional calculations. A comparison of the three species allows identification of the effect of the different number of valence electrons on the geometry of the complexes, on their electronic structure, and on the electronic transitions responsible for their absorption spectrum. In addition, a comparison between the dichloro derivative **3** and the previously studied pyridazine derivative $[Re_2(\mu\text{-Cl})_2(CO)_8(\mu\text{-pydz})]$ (**3pydz**)[8] allows assessment of the difference in the donor ability of the two heterocycles (ppd and pydz). Computational details can be found in the Experimental Section.

Optimized Geometry and Stability of the Complexes. The most relevant optimized geometrical parameters are reported in Table 1 (for a complete list, see Table S1 in the Supporting Information). For the three compounds, the

(25) For complex **3**, a small, irregular reduction peak connected with the oxidation peak is observed at a distance of about 0.3 V. Its features suggest accumulation on the electrode surface of the product of a chemical reaction following the electron loss. It is worthwhile comparing this case with the analogous phthalazine complex **3phal**, which gives a perfectly reversible bielectronic peak (working at 2 V s^{-1}, red line in Figure 3), gradually losing its chemical reversibility at lower scan rates. Now, the increasing competition of the chemical step with decreasing scan rate (such as in the 0.2 V s^{-1} characteristics, black line) results in a decreasing "regular" return peak and an increasing "irregular" one (in the same position as in the ppd complex case), corresponding to the reduction of the locally accumulated product of the chemical reaction.

Table 4. Calculated Dissociation (D_e), Interaction (ΔE_{int}), and Preparation (ΔE_{prep}) Energies [kJ mol^{-1}] for the Complexes [$Re_2(\mu\text{-}X)_2(CO)_6(\mu\text{-ppd})$] (**1**−**3**) and for [$Re_2(\mu\text{-}Cl)_2(CO)_6(\mu\text{-pydz})$] (**3pydz**)

	1	**2**	**3**	**3pydz**
D_e	237	212	192	240
ΔE_{int}	−263	−263	−264	−283
$\Delta E_{prep,M}$	13	34	40	42
$\Delta E_{prep,L}$	13	17	32	1

optimized geometry compares well to the corresponding solid-state structure as determined by X-ray diffraction.[26]

The minimum energy structure optimized for compounds **1**−**3** belongs to the C_s point group.[27] Deviation from the highest possible symmetry (C_{2v}) for species **1** and **3** is associated with the rotation of the two phenyl rings (in the same direction) out of the plane of the oxadiazole ring, in order to avoid their interaction with the equatorial carbonyl ligands. For compound **2**, the presence of two different bridging ligands (H and Cl) allows differentiation of the equatorial carbonyls. In particular, the carbonyl groups *cis* to the chloro ligand, due to the larger size of chlorine with respect to hydrogen, are more pushed toward the oxadiazole moiety. As a result the two phenyl rings rotate in such a way to avoid their interaction with these specific ligands.

The distortion from planarity of the 2,5-diphenyloxadiazole moiety connected with the bending of the rhenium-centered octahedra toward the nitrogen atoms of the bridging heterocyclic ligand increases on going from **1** to **2** to **3**, as already described in the X-ray structure characterization section. It is important to note, however, that the unfavorable steric interactions between the equatorial carbonyl ligands and oxadiazole does not lead to a restricted rotation of the phenyl rings. Indeed, the rotational barriers estimated for **1** and **3** (14.5 and 10.3 kJ mol^{-1}, respectively)[28] are lower than that computed for the free ligand (28.0 kJ mol^{-1}). This seemingly unexpected finding can be understood considering that steric hindrance affects the minimum energy portion of the rotational profile only while it has almost no effect on the transition structure. This result is in agreement with the dynamic symmetry shown by the phenyl rings in the ^{1}H NMR spectra of the complexes.

The dissociation energy D_e calculated for the complexes **1**−**3** and **3pydz** is reported in Table 4, along with its partition into three components: the (instantaneous) interaction energy, ΔE_{int}, and the preparation energies, $\Delta E_{prep,M}$ and $\Delta E_{prep,L}$.[29] The interaction energy is the energy difference between the complex (ML) and the constituting fragments (M and L) computed employing the frozen geometry of the complex. The preparation energy (also known as deformation energy) is the energy necessary to promote the (metal or ligand) fragment from its equilibrium geometry to the geometry adopted in the complex.

(26) Mean and maximum absolute deviations in bond distances (1.7 and 3.7 pm) and bond angles (0.7° and 2.3°) are small, particularly if the standard deviations of the experimental data are taken into account.
(27) Higher energy conformers belonging to different point groups have been characterized for **1** and **3** (see the Experimental Section).
(28) Rotational barriers have been estimated optimizing a C_s-symmetric structure in which one of the two phenyl rings lays on a plane orthogonal to the oxadiazole ring.
(29) The dissociation energy is the opposite of the sum of the three terms: $-D_e = \Delta E_{int} + \Delta E_{prep,M} + \Delta E_{prep,L}$. Zhang, J.; Frenking, G. *Chem. Phys. Lett.* **2004**, *394*, 120–125.

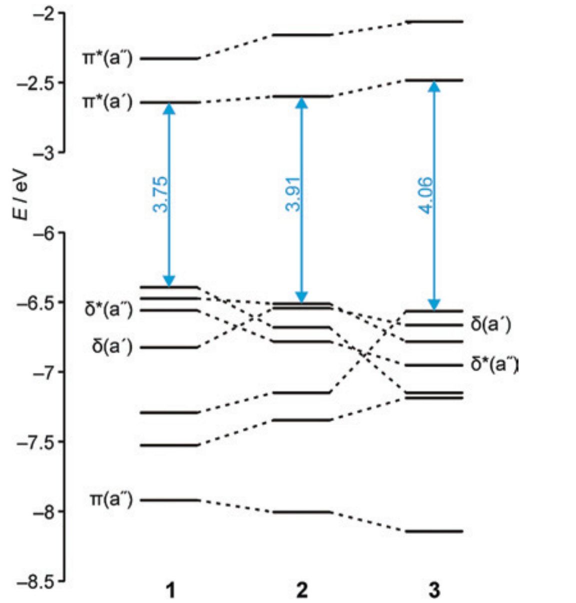

Figure 4. Partial molecular orbital diagrams for the C_s-symmetric oxadiazole complexes **1**−**3**. Blue arrows highlight HOMO−LUMO gaps (DFT energy values in eV are given).

The computed dissociation energy decreases on going from **1** to **2** to **3**, in agreement with the observed kinetic stability of the complexes in acetonitrile solution. However, the interaction energy is almost identical for the three species and the difference in stability can be entirely attributed to differences in the preparation energy of both the metal and the 2,5-diphenyloxadiazole fragments. These findings are in accord with the trend observed in the above-described geometrical distortions (i.e., the bending of the rhenium-centered octahedra and the loss of planarity of the ppd ligand) and is consistent with a similar donation from the ppd ligand to the metal atoms in the three compounds.

As far as the two dichloro derivatives **3** and **3pydz** are concerned, the greater dissociation energy computed for the pyridazine complex is in agreement with its experimental higher stability in acetonitrile solution. The stability of **3pydz** can be attributed both to a higher interaction energy and to a lower preparation energy for the ligand fragment (almost zero for **3pydz**). This is expected, since pyridazine, being richer in electrons than oxadiazole, acts as a better ligand toward the metal fragment and no substantial difference between the geometry of the free and the coordinated pyridazine can be detected. The preparation energy for the metal fragment in the two complexes is similar, since the bite of the two bridging ligands, albeit not identical, leads to a superimposable geometry of the [$Re_2(\mu\text{-}Cl)_2(CO)_6$] fragment in the two complexes.

Electronic Structure and Transitions. Partial molecular orbital diagrams for the C_s-symmetric oxadiazole complexes here investigated are reported in Figure 4, while isodensity surface plots of some relevant molecular orbitals are depicted in Figures 5 and 6.

The two lowest unoccupied molecular orbitals (LUMO and LUMO + 1) correspond to the two lowest-lying π^* orbitals

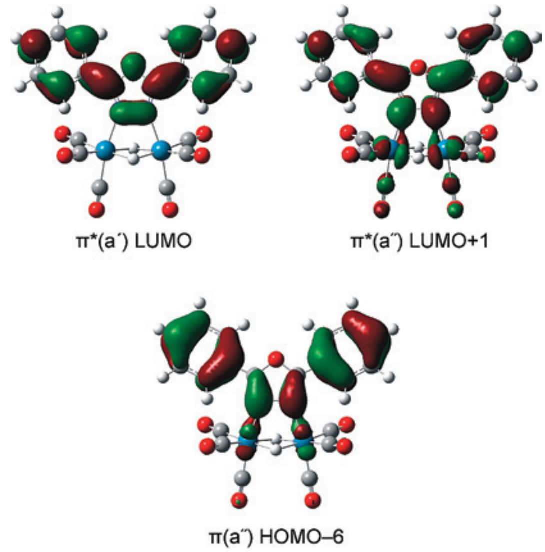

Figure 5. Isodensity surface plots of some relevant molecular orbitals of $[Re_2(\mu\text{-}H)_2(CO)_6(\mu\text{-ppd})]$ (**1**) mainly located on the diphenyloxadiazole ligand. The corresponding molecular orbitals for molecules **2** and **3** are very similar.

of the diphenyloxadiazole molecule. In Figures 4 and 5, they are indicated by $\pi^*(a')$ and $\pi^*(a'')$, according to their symmetry labels. As expected, as a consequence of the coordination to the rhenium atoms, the reduced electron density on the ligand ring leads to an overall stabilization of the two orbitals with respect to the free ligand (in which they lie at -1.51 and -0.69 eV, respectively).[30] On going from **1** to **2** to **3**, their energy significantly rises. This effect can be safely attributed to the increasing distortion of the ppd ligand, the two orbitals being π-bonding with respect to the C(oxadiazole)−C(phenyl) interaction (see Figure 5, first row). This explanation is supported by computations on the free oxadiazole ligand, showing an analogous raising of the LUMO energy on displacing the phenyl groups from the plane of the heterocyclic ring.[31]

Within the highest occupied molecular orbitals of the three complexes, HOMO − 6 corresponds to the HOMO of the free ligand, indicated by $\pi(a'')$ in Figures 4 and 5. This orbital too is stabilized as a consequence of coordination (it lies at -6.41 eV in free ppd). However, due to its π-antibonding nature with respect to the C(oxadiazole)−C(phenyl) interaction, its energy lowers on going from **1** to **2** to **3**.

The six HOMOs correspond to the in-phase and out-of-phase combinations of the "t_{2g}" sets of the two rhenium atoms in a pseudo-octahedral coordination environment. For the unsaturated derivative **1**, the two bridging hydrido ligands give no contribution to these orbitals (see Figure 6, first column). The three Re−Re bonding (a' symmetry) and the three Re−Re antibonding (a'' symmetry) molecular orbitals can be found in order of increasing energy, spanning an energy range of 1.13 eV. Moving to **2** and **3**, the Re−Re distance strongly lengthens, and as a consequence, the energy range covered by these increasingly Re−Re nonbonding orbitals contracts to 0.84 and 0.63 eV (for **2** and **3**, respectively). However, this general trend (the destabilization of the a' orbitals and the stabilization of the a'' orbitals) is complicated by the presence of the bridging chloro ligands whose occupied p orbitals can interact with the d orbitals of the metal atoms leading to a Re−Cl π-antibonding character for some of the HOMOs in **2** and **3** (see Figure 6, second and third columns).

In Figure 6, three orbitals are depicted, namely, the HOMO (connected to the reduction potential of these complexes) and the two orbitals with δ symmetry with respect to the Re−Re interaction, indicated by $\delta^*(a'')$ and $\delta(a')$ (involved in the MLCT transitions). The nature of the HOMO changes on going from the dihydrido derivative **1** (in which it shows a substantial Re−Re antibonding character) to the hydridochloro derivative **2** (in which a small Re−Cl antibonding character is present) to the dichloro derivative **3** (which is all-antibonding with respect to the four Re−Cl interactions). The HOMO energy trend within this series cannot be easily predicted since two competitive effects (the lengthening of the Re−Re distance and the build-up of a Re−Cl antibonding character) are at work. However, the increasing HOMO−LUMO energy gap computed along the series well compares with the trend determined by the electrochemical experiments.

The out-of-phase combination of rhenium orbitals δ^*, due to its a'' symmetry, cannot combine with the chlorine p orbitals, and its energy strongly lowers along the **1**−**3** series as expected. Due to the antibonding contribution of the p orbitals of the chlorine atoms, the opposite trend is shown by the in-phase combination of rhenium orbitals δ.

In order to simulate the absorption electronic spectrum of the oxadiazole complexes down to 250 nm, the lowest 30 singlet excitation energies were computed. However, only singlet excitations for which the oscillator strength f is greater than 0.01 are reported in Table 5 and depicted in Figure 2. Computations have been done both in the gas-phase and in dichloromethane solution (employing the conductor-like polarizable continuum model CPCM) in order to evaluate the solvent effect. As expected, the CPCM results are significantly different from the gas-phase results for the MLCT transitions only, while the $\pi-\pi^*$ transitions centered on the ppd ligand are somehow unaffected by the solvent.

The orbitals involved in the $\pi-\pi^*$ transitions are the HOMO − 6 $\pi(a'')$ and the LUMO $\pi^*(a')$.[32] The $\pi-\pi^*$ transition for the three complexes is blue-shifted with respect to the free ligand[33] and its wavelength lowers along the series

(30) A list of molecular orbital energies for the oxadiazole ligand and the three rhenium complexes **1**−**3** can be found in Table S2 (Supporting Information).

(31) The effect of phenyl ring rotation (within imposed C_s symmetry) on the computed HOMO and LUMO energy, HOMO−LUMO energy gap, excitation energy, and oscillator strength for the $\pi-\pi^*$ transition can be found in the Supporting Information (Table S3 and Figures S2 and S3). Similar computations, albeit limited to the HOMO−LUMO gap, can be found in ref 21.

(32) In Table 5, two entries are listed in correspondence to the transition since, mainly for the dichloro derivative **3**, a phenyl ring centered orbital of a'' symmetry (HOMO − 8), lying close to the HOMO − 6 (a''), contributes to these type of transitions. A complete list of the contribution of singly excited configurations to all the electronic transitions described in the text can be found in the Supporting Information (Table S4).

(33) Values computed for the diphenyloxadiazole molecule: gas-phase $\lambda_{\pi-\pi^*}$ = 289 nm (4.29 eV), f = 0.87; dichloromethane solution (CPCM) $\lambda_{\pi-\pi^*}$ = 294 nm (4.22 eV), f = 0.97.

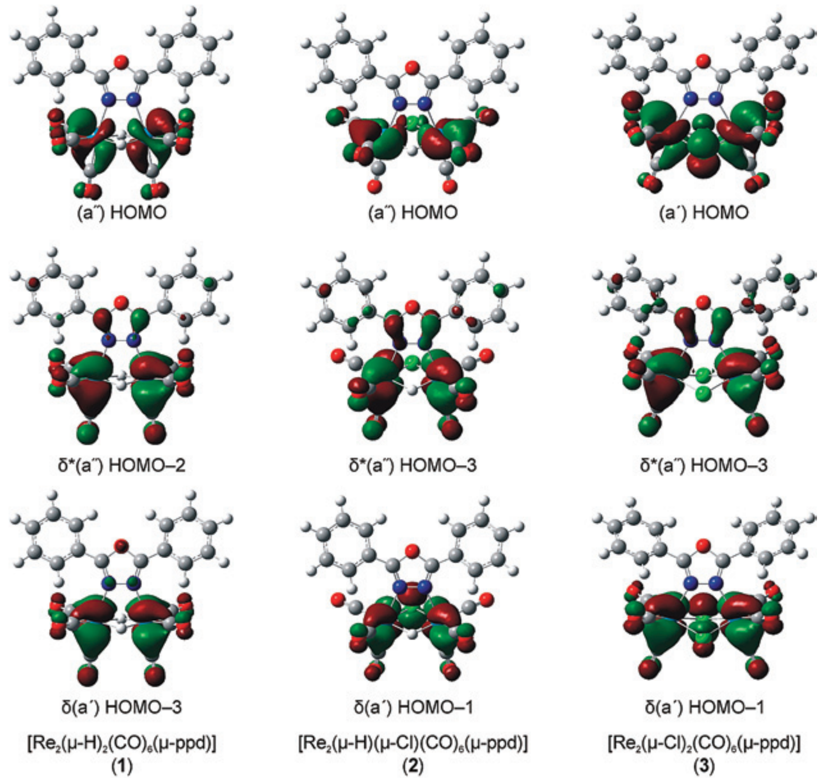

Figure 6. Isodensity surface plots of some relevant molecular orbitals of $[Re_2(\mu\text{-}X)_2(CO)_6(\mu\text{-ppd})]$ (**1**−**3**) mainly located on the $Re_2(\mu\text{-}X)_2$ core (top row HOMO; middle row δ*; bottom row δ).

Table 5. Computed Excitation Energies and Oscillator Strengths for the Complexes $[Re_2(\mu\text{-}X^1)(\mu\text{-}X^2)(CO)_6(\mu\text{-ppd})]$ (**1**−**3**)

	1	2	3
		Gas-Phase Values	
$\lambda_{\pi-\pi^*}$ [nm, eV] (f)	266, 4.66 (0.02)	261, 4.75 (0.03)	255, 4.87 (0.27)
	272, 4.55 (0.51)	267, 4.65 (0.45)	257, 4.83 (0.13)
λ_{MLCT} [nm, eV] (f)	354, 3.51 (0.01)	324, 3.82 (0.13)	303, 4.09 (0.13)
	358, 3.46 (0.11)	350, 3.54 (0.05)	322, 3.85 (0.09)
	370, 3.35 (0.11)	362, 3.42 (0.02)	339, 3.66 (0.01)
	385, 3.22 (0.04)	390, 3.18 (0.02)	365, 3.40 (0.02)
		Dichloromethane Solution Values (CPCM)	
$\lambda_{\pi-\pi^*}$ [nm, eV] (f)	267, 4.65 (0.05)	264, 4.70 (0.04)	254, 4.89 (0.33)
	273, 4.55 (0.52)	265, 4.68 (0.43)	257, 4.82 (0.15)
λ_{MLCT} [nm, eV] (f)	318, 3.90 (0.09)	307, 4.03 (0.20)	283, 4.38 (0.14)
	336, 3.69 (0.02)	320, 3.87 (0.16)	295, 4.20 (0.21)
	343, 3.61 (0.09)	331, 3.75 (0.02)	310, 4.00 (0.04)
	357, 3.47 (0.17)	341, 3.64 (0.03)	322, 3.85 (0.03)

1−**3**. These findings are a consequence of the above-described changes in energy of the two orbitals and are well reproduced by computations on the (distorted) free oxadiazole molecule (see Table S3 and Figure S3 in the Supporting Information).

The orbitals involved in the MLCT transitions are the above-described $\delta(a')$ and $\delta^*(a'')$ HOMOs and the two LUMOs $\pi^*(a')$ and $\pi^*(a'')$. Hence, four singly excited configurations must be taken into account, two of A′ and two of A″ symmetry. They are differently combined to give the four transitions listed in Table 5. The MLCT excitation energies show a strong blue shift along the **1**−**3** series. However, since the molecular orbitals $\delta^*(a'')$ and $\pi^*(a'')$, involved in the more intense MLCT transitions, move more than the orbitals $\pi(a'')$ and $\pi^*(a')$, involved in the $\pi-\pi^*$ transitions, the MLCT band is substantially more blue-shifted than the $\pi-\pi^*$ band along the series, and for compound **3**, the MLCT component can only be detected as a shoulder of the intraligand band (see Figure 2).

Conclusions

This work provides the first detailed study of the properties of 2,5-diphenyl-1,3,4-oxadiazole as a ligand toward transition metal centers. It has been shown that these molecules are able to act as bridging ligands, through the two nitrogen atoms, toward $Re_2(\mu\text{-}X)_2(CO)_6$ fragments spanning a wide range of intermetallic distances (from 278 to 358 pm). The stability of the oxadiazole complexes is lower than that of the corresponding 1,2-diazine derivatives, but it is high enough to allow isolation in the solid state and also characterization in solution. On the basis of the density functional computations, the lower stability with respect to the diazine complexes is attributable not only to the lower donating ability of the more electron-poor oxadiazole but also to the significant geometrical reorganization imposed by this sterically demanding ligand.

As expected, coordination makes oxadiazole reduction easier. However, the positive shift of the reduction potential upon coordination is much lower than in the case of the corresponding complexes with bridging 1,2-diazines. This is probably a further indication of the lower donor power of the oxadiazole system. A similar effect was previously observed in the analogous 1,2-diazine complexes, where the introduction of electron-withdrawing substituents lowered the coordination shift of the reduction potential (E_{red} values: pydz, free −2.60 V, bound −1.35 V, shift +1.25 V; 3,6-Cl_2pydz, free −1.99 V, bound −0.99 V, shift +1.00 V).

Coordination very effectively quenches emission from oxadiazole indicating fast radiationless relaxation to low-energy states arising from the presence of the d orbitals of the heavy metal atoms, which also enhance, by spin−orbit coupling, the rate of formally spin-forbidden processes. However, the emission from the ^{3}MLCT states is absent (or very low), probably because the low basicity and the bulk of diphenyloxadiazole reduce the stiffness of the molecular structure, favoring nonradiative de-excitation pathways.

The observed photoinstability might be related to an increased steric interaction between ppd and the metallic fragment in the excited state with respect to the ground state. Indeed, in the excited state a backward displacement of ppd toward planarity is expected (due to the π bonding character of the LUMO about the C(oxadiazole)−C(phenyl) bond), as well as a shortening of the Re−N bond distance (due to charge separation). This would lead to excessive steric hindrance, and the effect should be more sizable for the dichloro derivative, in accord with the larger deviation from planarity of ppd in this species.

Coordination therefore has a detrimental effect on the emitting properties of oxadiazoles, but a beneficial outcome on their electrochemical properties, due to the lowering of the reduction potentials. Then the coordination of diaryloxadiazoles to metal centers could improve their electron transporting properties, at least insofar as they are affected by the LUMO energies. So these results suggest focusing future search on the coordination to metal centers with higher Lewis acidity (to counterbalance the low basicity of oxadiazoles) and with smaller coordination number than octahedral rhenium(I).

Experimental Section

All reactions were performed under N_2 using the Schlenk technique. All of the solvents were deoxygenated and dried by standard methods. 2,5-Diphenyl-1,3,4-oxadiazole (ppd) was used as received from Fluka. $[Re_4(\mu_3\text{-}H)_4(CO)_{12}]\cdot 2C_6H_6$ and $[ReCl(CO)_5]$ were prepared according to literature methods.[34,35] ^{1}H NMR spectra were recorded on Bruker DRX300 or DRX400 spectrometers. IR spectra were acquired on a Bruker Vector22 FT instrument. Electronic absorption spectra were recorded on a Jasco V-570 spectrophotometer at room temperature. Steady-state fluorescence measurements were performed with a Jobin-Yvon Fluorolog-3 spectrometer equipped with double monochromators and a Hamamatsu R928P photomultiplier tube as a detector. All the solutions were deaerated by nitrogen bubbling for 30 min before measurements. Emission quantum yield of **2** has been determined by comparison with the emission of quinine sulfate in H_2SO_4, 0.1 M (0.577).[36]

Synthesis of $[Re_2(\mu\text{-}H)_2(CO)_6(\mu\text{-ppd})]$ (1). A solution of $[Re_4(\mu_3\text{-}H)_4(CO)_{12}]\cdot(C_6H_6)_2$ (112 mg, 0.090 mmol) in CH_2Cl_2 (20 mL) was treated at room temperature with 2 equiv of ppd (40.0 mg, 0.18 mmol). The color slowly changed from red-brown to lemon yellow, followed by slow separation of a yellow precipitate.

Table 6. Spectroscopic Data for the New Complexes **1**−**3** and the Free Ligand[a]

	ν(CO) [cm^{-1}]	δ [ppm]
ppd		8.19 (m, 4H), 7.60 (m, 6H)
1	2042m, 2016s, 1939sh, 1927vs	8.54 (m, 4H), 7.90 (m, 2H), 7.79 (m, 4H)
2	2048m, 2027s, 1947s, 1921s	8.30 (m, 4H), 7.88 (m, 2H), 7.78 (m, 4H)
3	2051mw, 2036s, 1946s, 1917s	8.17 (m, 4H), 7.89 (m, 2H), 7.79 (m, 4H)

[a] IR bands in CH_2Cl_2 and ^{1}H NMR resonances of the ppd moiety in CD_2Cl_2.

The solution was stirred overnight; then the volume was reduced to $^1/_5$, and the solution was treated with *n*-hexane, causing the precipitation of a yellow powder, which was washed with CH_2Cl_2 (2 mL) to completely remove byproducts. The residue was dried under vacuum, affording 98 mg (0.128 mmol) of pure **1** (isolated yield 71%). Elemental Anal. Calcd for $C_{20}H_{12}N_2O_7Re_2$: C 31.41, H 1.58, N 3.66. Found: C 31.47, H 1.65, N 3.60. IR and NMR data are summarized in Table 6. Crystals for photophysical measurements and for X-ray analysis were obtained by slow diffusion of *n*-hexane into a CH_2Cl_2 solution at 248 K.

Synthesis of $[Re_2(\mu\text{-}H)(\mu\text{-}Cl)(CO)_6(\mu\text{-ppd})]$ (2). A sample of complex **1** (53.4 mg, 0.0698 mmol) was dissolved in CH_2Cl_2 (15 mL), and the solution was treated with 10 mL of a saturated solution of HCl in CH_2Cl_2. The mixture was stirred at room temperature for 4 h, during which time color changed from yellow to colorless. The solution was then concentrated, and the addition to *n*-hexane afforded the precipitation of a white powder. Isolated yield: 42.8 mg (0.0535 mmol, 77%). Elemental Anal. Calcd for $C_{20}H_{11}ClN_2O_7Re_2$: C 30.06, H 1.39, N 3.50. Found: C 30.31, H 1.55, N 3.52. IR and NMR data are summarized in Table 6. Crystals for photophysical measurements and for X-ray analysis were obtained by slow diffusion of *n*-hexane into a CH_2Cl_2 solution at 248 K.

Synthesis of $[Re_2(\mu\text{-}Cl)_2(CO)_6(\mu\text{-ppd})]$ (3). A sample of $[ReCl(CO)_5]$ (41.3 mg, 0.114 mmol) was dissolved, upon heating, in freshly distilled toluene (20 mL). Then 0.5 equiv (12.7 mg, 0.0572 mmol) of ppd was added, and the solution was refluxed for 1.5 h. ^{1}H NMR showed the formation of one product only. Evaporation to dryness under vacuum gave a white residue, which was dissolved in CH_2Cl_2 and precipitated with *n*-hexane, affording microcrystalline pure **3**. Isolated yield: 38.2 mg (0.0458 mmol, 80%) Elemental Anal. Calcd for $C_{20}H_{10}Cl_2N_2O_7Re_2$: C 28.82, H 1.21, N 3.36. Found: C 28.90, H 1.23, N 3.30. IR and NMR data are summarized in Table 6. Crystals for photophysical measurements and for X-ray analysis were obtained by slow diffusion of *n*-hexane into a CH_2Cl_2 solution at 248 K.

Reaction between $[ReCl(CO)_5]$ and 1 equiv of ppd. A sample of $[ReCl(CO)_5]$ (64.2 mg, 0.177 mmol) was dissolved, upon heating, in freshly distilled toluene (20 mL). Then 1 equiv (39.3 mg, 0.177 mmol) of ppd was added, and the solution was refluxed for 4 h. IR and ^{1}H NMR showed the formation of **3** and the presence of unreacted ppd (in 1:1 ratio). The toluene solution was further refluxed for 8 h, but no changes in the IR spectrum were observed.

^{1}H NMR Monitoring of the Complex Stability in Acetonitrile. A series of spectra was recorded on a saturated solution of **1** in CD_3CN at room temperature for 21 h. The spectra showed the slow disappearance of **1** ($t_{1/2}$ = 13.6 h) with formation of free ppd and several unidentified hydrido species. At the beginning, the most important hydrido resonance was at δ −4.63 ppm, tentatively attributable to the derivative of substitution of ppd by CD_3CN, of formula $[Re_2(\mu\text{-}H)_2(CO)_6(CD_3CN)_2]$. This species further evolved, with partial H_2 loss and formation of many species. Among them, the known triangular cluster $[Re_3(\mu\text{-}H)_3(CO)_9(CD_3CN)_3]$ was identified.

(34) (a) Andrews, M. A.; Kirtley, S. W.; Kaesz, H. D. *Inorg. Chem.* **1977**, *16*, 1556–1561. (b) Johnson, J. R.; Kaesz, H. D. *Inorg. Synth.* **1978**, *18*, 60–62.
(35) Schmidt, S. P.; Trogler, W. C.; Basolo, F. *Inorg. Synth.* **1985**, *23*, 41–46.
(36) Lacowicz, J. R. *Principles of Fluorescence Spectroscopy*, 2nd ed.; Kluwer: New York, 1999.

A similar experiment was performed on a CD_3CN solution of **2**. In this case, the decomposition reaction was faster ($t_{1/2}$ = 4.5 h) and more selective, affording a main hydrido species only, responsible for a resonance at δ −9.13 ppm.

In the case of **3**, the progress of the reaction was monitored by the changes in the aromatic region, which showed the progressive decrease of concentration of **3** ($t_{1/2}$ = 3.7 h) accompanied by the corresponding formation of free ppd. The reaction was repeated in a Schlenk tube in MeCN at room temperature and monitored overnight by IR. At the end, the ν(CO) bands of **3** disappeared, replaced by bands attributable to *fac*-[ReCl(CO)$_3$(MeCN)$_2$] (2036s, 1933s, 1909s cm^{-1}). The solvent was removed under vacuum, and the residue dissolved in CH_2Cl_2. After 2 days, IR and NMR spectra showed that most of the monomeric complex had converted back into **3**.

Reaction of 3 with Tetrahydrofuran. The reaction was performed in a NMR tube employing THF-d_8 as a solvent. The ^{1}H NMR spectra, at 298 K, showed the progressive increase of the resonances of free ppd at the expense of **3**, with a slower kinetics than in the case of MeCN ($t_{1/2}$ = 17.2 h). The reaction was repeated in a Schlenk tube, in THF at room temperature: after 44 h the IR spectrum showed, besides the ν(CO) bands of **3**, also absorptions at 2026m, 1905s, and 1890s, attributable to [ReCl(CO)$_3$(THF)$_2$] for the close similarity to those of the corresponding Br derivative (2027s, 1910s, and 1892s).[37] ^{1}H NMR in $CDCl_3$ showed the resonances of free ppd.

Competition Experiment: Reaction of [ReCl(CO)$_5$] with ppd and pydz. A sample of [ReCl(CO)$_5$] (10.7 mg, 0.0295 mmol) was treated with 3.3 mg of ppd (0.0148 mmol) and 1 μL of pydz (0.0138 mmol) in 4 mL of freshly distilled toluene. The solution was heated at reflux for 1.5 h. A yellow color became detectable after 15 min. The IR and ^{1}H NMR spectra unambiguously revealed the formation of [Re$_2$(μ-Cl)$_2$(CO)$_6$(μ-pydz)] and the presence of unreacted ppd.

X-Ray Diffraction Structural Analysis. Data for **1**: $C_{20}H_{12}N_2O_7Re_2$, M = 764.72, triclinic, $P\bar{1}$ (No. 2), a = 8.121(2) Å, b = 11.430(2) Å, c = 12.526(2) Å, α = 98.52(2)°, β = 103.24(2)°, γ = 109.18(2)°, V = 1036.9(4) Å^3, Z = 2, D_x = 2.449 g cm^{-3}, λ(Mo Kα) = 0.71073 Å, μ = 11.708 mm^{-1}, F(000) = 704, T = 110(2) K, $R(F)$ = 0.0242, $R_w(F^2)$ = 0.0450.

Data for **2**·CH_2Cl_2: $C_{21}H_{13}Cl_3N_2O_7Re_2$, M = 884.08, triclinic, $P\bar{1}$ (No. 2), a = 8.483(2) Å, b = 12.283(2) Å, c = 13.447(2) Å, α = 63.14(2)°, β = 80.25(2)°, γ = 77.79(2)°, V = 1217.3(4) Å^3, Z = 2, D_x = 2.412 g cm^{-3}, λ(Mo Kα) = 0.71073 Å, μ = 10.310 mm^{-1}, F(000) = 820, T = 110(2) K, $R(F)$ = 0.0151, $R_w(F^2)$ = 0.0404.

Data for **3**: $C_{20}H_{10}Cl_2N_2O_7Re_2$, M = 833.60, monoclinic, $P2_1/c$ (No. 14), a = 9.100(2) Å, b = 13.758(2) Å, c = 18.517(2) Å, β = 93.12(2)°, V = 2314.9(7) Å^3, Z = 4, D_x = 2.392 g cm^{-3}, λ(Mo Kα) = 0.71073 Å, μ = 10.724 mm^{-1}, F(000) = 1536, T = 295(2) K, $R(F)$ = 0.0157, $R_w(F^2)$ = 0.0384.

Electrochemical Measurements. The cyclovoltammetric study of the complexes has been performed at scan rates typically ranging from 0.02 to 10 V s^{-1} in HPLC-grade MeCN solutions at 0.00025−0.001 M concentration in each substrate, deaerated by N_2 bubbling, with 0.1 M TBAPF$_6$ (Fluka) as the supporting electrolyte, at 298 K. The ohmic drop has been compensated by the positive feedback technique.[38] The experiments were carried out using an AUTOLAB PGSTAT potentiostat (EcoChemie, The Netherlands) run by a PC with GPES software. The working electrode was a glassy carbon one (AMEL, diameter = 1.5 mm) cleaned by diamond powder (Aldrich, diameter = 1 μm) on a wet cloth (STRUERS DP-NAP); the counter electrode was a platinum wire; the reference electrode was an aqueous saturated calomel electrode, having in our working medium a difference of −0.385 V vs the Fc$^+$|Fc couple (the intersolvent redox potential reference currently recommended by IUPAC)[39] and +0.032 V vs the Me$_{10}$Fc$^+$|Me$_{10}$Fc couple (an improved intersolvent reference under investigation).[40]

Computational Details. Geometries were optimized by means of density functional calculations. The parameter-free hybrid functional PBE0[41] was employed along with the standard valence double-ζ polarized basis set 6-31G(d,p) for C, H, Cl, N, and O. For Re, the Stuttgart−Dresden effective core potentials were employed along with the corresponding valence triple-ζ basis set. The effect of basis set expansion was previously checked studying an analogous pyridazine derivative[8] and found to be negligible.

All the calculations were done assuming C_s symmetry. The nature of all the stationary points was checked by computing vibrational frequencies, and all the species were find to be true minima. Higher energy conformers belonging to different point groups were found for **1** and **3**. In particular, a C_{2v}-symmetric conformer in which the diphenyloxadiazole ligand is planar was found for **1**, lying only 0.3 kJ mol^{-1} higher in energy with respect to the C_s minimum. A C_2-symmetric conformer in which the two phenyl rings are rotated in two opposite directions out of the oxadiazole plane was found for **3**, lying 7.7 kJ mol^{-1} higher in energy with respect to the C_s minimum. For compound **2**, any attempt to optimize a structure in which one or both the phenyl rings were rotated in the opposite direction with respect to that found in the minimum energy structure failed, and no other conformer can be found.

Dissociation and interaction energy values reported in Table 4 are counterpoise corrected.[42]

In order to simulate the absorption electronic spectrum down to 250 nm, the lowest 30 singlet excitation energies were computed by means of time-dependent density functional calculations.

(37) D'Alfonso, G. Unpublished results. See also: Vitali, D.; Calderazzo, F. *Gazz. Chim. Ital.* **1972**, *102*, 587–596.
(38) Bard, A. J.; Faulkner, L. R. *Electrochemical Methods. Fundamentals and Applications*; Wiley: New York, 2002; pp 648−650.
(39) (a) Gritzner, G.; Kuta, J. *Pure Appl. Chem.* **1984**, *56*, 461–466. (b) Gritzner, G. *Pure Appl. Chem.* **1990**, *62*, 1839–1858.
(40) (a) Falciola, L.; Gennaro, A.; Isse, A. A.; Mussini, P. R.; Rossi, M. *J. Electroanal. Chem.* **2006**, *593*, 47–56.
(41) Called PBE1PBE in Gaussian: (a) Adamo, C.; Barone, V. *J. Chem. Phys.* **1999**, *111*, 6158–6170. (b) Perdew, J. P.; Burke, K.; Ernzerhof, M. *Phys. Rev. Lett.* **1996**, *77*, 3865–3868. (c) Perdew, J. P.; Burke, K.; Ernzerhof, M. *Phys. Rev. Lett.* **1997**, *78*, 1396.
(42) Kestner, N. R.; Combariza, J. E. In *Reviews in Computational Chemistry*; Lipkowitz, K. B., Boyd, D. B., Eds.; Wiley-VCH: New York, 1999; Vol. *13*, pp 99−132.
(43) (a) Barone, V.; Cossi, M. *J. Phys. Chem. A* **1998**, *102*, 1995–2001. (b) Cossi, M.; Barone, V. *J. Chem. Phys.* **2001**, *115*, 4708–4717. (c) Cossi, M.; Rega, N.; Scalmani, G.; Barone, V. *J. Comput. Chem.* **2003**, *24*, 669–681.
(44) Frisch, M. J.; Trucks, G. W.; Schlegel, H. B.; Scuseria, G. E.; Robb, M. A.; Cheeseman, J. R.; Montgomery, J. A., Jr.; Vreven, T.; Kudin, K. N.; Burant, J. C.; Millam, J. M.; Iyengar, S. S.; Tomasi, J.; Barone, V.; Mennucci, B.; Cossi, M.; Scalmani, G.; Rega, N.; Petersson, G. A.; Nakatsuji, H.; Hada, M.; Ehara, M.; Toyota, K.; Fukuda, R.; Hasegawa, J.; Ishida, M.; Nakajima, T.; Honda, Y.; Kitao, O.; Nakai, H.; Klene, M.; Li, X.; Knox, J. E.; Hratchian, H. P.; Cross, J. B.; Bakken, V.; Adamo, C.; Jaramillo, J.; Gomperts, R.; Stratmann, R. E.; Yazyev, O.; Austin, A. J.; Cammi, R.; Pomelli, C.; Ochterski, J. W.; Ayala, P. Y.; Morokuma, K.; Voth, G. A.; Salvador, P.; Dannenberg, J. J.; Zakrzewski, V. G.; Dapprich, S.; Daniels, A. D.; Strain, M. C.; Farkas, O.; Malick, D. K.; Rabuck, A. D.; Raghavachari, K.; Foresman, J. B.; Ortiz, J. V.; Cui, Q.; Baboul, A. G.; Clifford, S.; Cioslowski, J.; Stefanov, B. B.; Liu, G.; Liashenko, A.; Piskorz, P.; Komaromi, I.; Martin, R. L.; Fox, D. J.; Keith, T.; Al-Laham, M. A.; Peng, C. Y.; Nanayakkara, A.; Challacombe, M.; Gill, P. M. W.; Johnson, B.; Chen, W.; Wong, M. W.; Gonzalez, C.; Pople, J. A. *Gaussian 03*, revision D.01; Gaussian Inc., Wallingford, CT, 2004.

Calculations were done also in the presence of solvent (dichloromethane, used in most of the photophysical characterizations) described by the conductor-like polarizable continuum model (CPCM).[43]

All the calculations were done with Gaussian 03.[44]

Acknowledgment. We thank Italy's MIUR for financial support (FIRB 2003, RBNE033KMA, Molecular compounds and hybrid nanostructured material with resonant and non resonant optical properties for photonic devices, and PRIN2007, Aggregation and functionalization of clusters: an opportunity for new materials).

Supporting Information Available: Experimental and optimized geometries, molecular orbital energies, composition and energy of the computed electronic transitions, plots of various properties of the free ligand as a function of the phenyl ring rotation, and the emission spectra of **3** upon successive excitations. This material is available free of charge via the Internet at http://pubs.acs.org.

IC801447Z